nature neuroscience

A new mode of corticothalamic transmission revealed in the *Gria4*$^{-/-}$ model of absence epilepsy

Jeanne T Paz[1], Astra S Bryant[1], Kathy Peng[1], Lief Fenno[2], Ofer Yizhar[2], Wayne N Frankel[3], Karl Deisseroth[2] & John R Huguenard[1]

Cortico-thalamo-cortical circuits mediate sensation and generate neural network oscillations associated with slow-wave sleep and various epilepsies. Cortical input to sensory thalamus is thought to mainly evoke feed-forward synaptic inhibition of thalamocortical (TC) cells via reticular thalamic nucleus (nRT) neurons, especially during oscillations. This relies on a stronger synaptic strength in the cortico-nRT pathway than in the cortico-TC pathway, allowing the feed-forward inhibition of TC cells to overcome direct cortico-TC excitation. We found a systemic and specific reduction in strength in GluA4-deficient (*Gria4*$^{-/-}$) mice of one excitatory synapse of the rhythmogenic cortico-thalamo-cortical system, the cortico-nRT projection, and observed that the oscillations could still be initiated by cortical inputs via the cortico-TC-nRT-TC pathway. These results reveal a previously unknown mode of cortico-thalamo-cortical transmission, bypassing direct cortico-nRT excitation, and describe a mechanism for pathological oscillation generation. This mode could be active under other circumstances, representing a previously unknown channel of cortico-thalamo-cortical information processing.

Cortico-thalamo-cortical circuits mediate sensation, perception and consciousness, and generate neural network oscillations associated with physiological sleep-spindle activity and focal or generalized epileptic activities such as absence seizures[1–3]. Communication between cerebral cortex and thalamic relay nuclei is mediated by reciprocally connected corticothalamic (CT) and TC glutamatergic excitatory pathways. Cortical input is thought to influence primary sensory thalamus by a feed-forward synaptic inhibition of TC relay neurons by GABAergic nRT or perigeniculate neurons[4–9]. CT neurons excite nRT neurons, which subsequently inhibit TC relay neurons. Cortico-thalamo-cortical oscillations are initiated if this inhibition is followed by post-inhibitory rebound bursts of action potentials in TC neurons that in turn re-excite nRT neurons. As this sequence iterates, a network oscillation is sustained[3,6,7,10]. These events in the thalamus, which is an important element in the generation of neural oscillations in cortico-thalamo-cortical circuits, rely on a stronger synaptic excitation in the CT-nRT than in the CT-TC pathway, allowing the inhibition of TC cells to overcome direct CT-TC excitation[7]. GluA4 AMPA receptors are more strongly expressed in thalamus versus neocortex[11,12] and, to a greater extent on nRT than on TC cells, providing a basis for such differences in synaptic strength[13]. GluA4 receptors should therefore be critical for information transfer from cortex to thalamus and, notably, in initiating and/or sustaining oscillations in the cortico-thalamo-cortical loop. We found that, paradoxically, *Gria4*$^{-/-}$ mice exhibited absence seizures and thalamic hyperexcitability.

We dissected the cellular and network mechanisms in the rhythmogenic thalamic component of the cortico-thalamo-cortical system that result in network hyperexcitability. Such dissection of synaptic pathways is challenging because cortex and thalamus are reciprocally connected and their axons are adjacent; thus, a selective stimulation of CT or TC axons is impossible with electrical stimulation, which activates both pathways. We overcame this difficulty by expressing channelrhodopsin-2 (ChR2), a light-sensitive cation channel[14], in either CT or TC neurons. ChR2 expression enables somata and axons to be activated by blue light with a high temporal precision[15–19].

RESULTS

GluA4 deficiency enhances thalamocortical oscillations

We assessed the electroencephalographic phenotype of *Gria4*$^{-/-}$ mice by performing electroencephalographic (EEG) recordings in freely moving animals. All of the *Gria4*$^{-/-}$ mice ($n = 5$) exhibited spontaneous spike-and-wave discharges (SWDs) associated with a behavioral arrest (**Fig. 1a**,**b**), consistent with previous findings in *Gria4*$^{-/-}$ and hypomorphic mutant mice[20]. The intra-SWD frequency, revealed by spectral analysis of the EEG signals, ranged from 5–9 Hz (**Fig. 1c**). SWDs ($n = 290$) recorded from five *Gria4*$^{-/-}$ mice occurred once every minute and had a variable duration (1–30 s). Systemic injection of ethosuximide (ETX), a first choice anti-absence drug, abolished SWDs in two of three mice (**Fig. 1d**). In one mouse, SWD frequency was reduced, from 0.5 per min to 0.2 per min. SWD activity resumed 40–51 min following ETX treatment (recovery, 0.6 ± 0.3 SWDs per min, mean ± s.e.m.; pretreatment, 0.9 ± 0.3 SWDs per min, $n = 3$ mice; $P > 0.5$). Vehicle injection did not affect SWD recurrence frequency (pretreatment, 0.7 ± 0.2 SWDs per min; saline, 1.6 ± 1.0 SWDs per min, $n = 3$ mice; $P > 0.4$; **Fig. 1d**).

To investigate the effects of GluA4 deficiency on thalamic circuit function, we examined the properties of evoked thalamic oscillations.

[1]Department of Neurology and Neurological Sciences, Stanford University School of Medicine, Stanford, California, USA. [2]Department of Bioengineering, Stanford University School of Medicine, Stanford, California, USA. [3]The Jackson Laboratory, Bar Harbor, Maine, USA. Correspondence should be addressed to J.R.H. (john.huguenard@stanford.edu).

Received 24 November 2010; accepted 28 June 2011; published online 21 August 2011; doi:10.1038/nn.2896

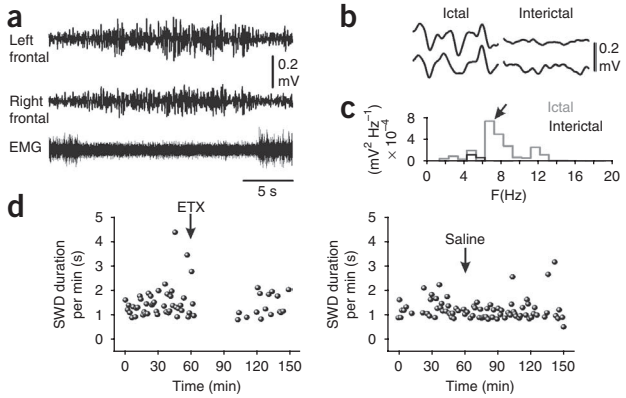

Figure 1 *Gria4*$^{-/-}$ mice display spontaneous SWDs. (**a**) EEG recordings from a *Gria4*$^{-/-}$ mouse, showing differential traces from two electrodes, over the right frontal and left frontal surfaces of the cerebral cortex. SWD occurrence in the EEG was associated with a reduced electromyographic (EMG) activity. (**b**) Representative 400-ms-long ictal and interictal EEG recordings. (**c**) Power spectrum of ictal (gray) and interictal (black) EEG activities (from left frontal trace). Arrow indicates the dominant frequency of the ictal EEG signal. (**d**) Plots of SWD duration and incidence from a *Gria4*$^{-/-}$ mouse, treated with either 200 mg per kg ethosuximide (ETX, left) or saline solution (0.9% NaCl, right), injected intraperitoneally after 60 min of recording (arrows). Cessation of SWDs post-injection was seen only in the ETX-treated mouse, followed by a recovery of SWD activity (1-min bins).

In horizontal thalamic slices, electrical stimulation of the internal capsule evoked rhythmic activity in the thalamus (**Fig. 2a**), consistent with previous findings[21,22]. Despite the absence of GluA4, the duration of evoked rhythmic activity was increased in thalamic slices from *Gria4*$^{-/-}$ mice compared with wild type (*Gria4*$^{-/-}$, 1.11 ± 0.16 s, $n = 7$ slices; wild type, 0.40 ± 0.18 s, $n = 8$ slices; $P < 0.05$; **Fig. 2**). These findings indicate that the absence of GluA4 results, paradoxically, in a hyperexcitable thalamic network.

GluA4 deficiency reduces spontaneous excitation in nRT

To determine whether the absence of GluA4 affected the synaptic activity of nRT GABAergic neurons, we examined spontaneous excitatory postsynaptic currents (sEPSCs, see Online Methods) in cells from wild-type and *Gria4*$^{-/-}$ mice. Despite the loss of this major AMPA receptor, electrophysiological recordings detected sEPSCs in all of the nRT neurons (16 of 16 neurons from 12 *Gria4*$^{-/-}$ mice; **Fig. 3**). However, the mean frequency of sEPSCs was reduced twofold in nRT neurons from *Gria4*$^{-/-}$ mice compared with wild type (**Fig. 3a**,**b**,**f**). We analyzed the characteristics of isolated sEPSCs in nRT neurons from wild-type ($n = 20$ cells) and *Gria4*$^{-/-}$ ($n = 16$ cells) mice. In both wild-type and *Gria4*$^{-/-}$ mice, sEPSCs were characterized by fast activation kinetics (**Fig. 3c**,**d**,**f**). In *Gria4*$^{-/-}$ mice, the amplitude of sEPSCs was reduced (~18%; **Fig. 3c**,**f**). Moreover, decay kinetics were slower in *Gria4*$^{-/-}$ nRT neurons, as measured as both the sEPSC weighted bi-exponential decay-time constant ($\tau_{D,W}$) and the half-width (**Fig. 3c**,**d**,**f**). These alterations in sEPSC frequency, amplitude and kinetics were observed across all populations of events, as demonstrated by the cumulative probability histograms (**Fig. 3e**).

In contrast with nRT neurons, sEPSCs in TC cells were unaffected by *Gria4* deficiency in terms of amplitudes and kinetics (**Supplementary Fig. 1**) and their frequency was not reduced (data not shown). These results indicate that the absence of GluA4 reduces spontaneous excitatory transmission in nRT, but not in TC, neurons. We then used an optogenetic approach to determine whether the reduced sEPSCs in nRT were the result of a reduced synaptic strength at CT-nRT, TC-nRT and/or CT-TC synapses.

GluA4 deficiency does not affect EPSCs at TC-nRT synapses

First we examined the TC-nRT pathway by expressing ChR2-containing virus in neurons in the ventrobasal complex (VB) of somatosensory thalamus, which is functionally connected to the somatosensory cortex[19,23–25]. We injected in VB thalamus with a virus carrying a transgene encoding a ChR2–enhanced yellow fluorescent protein (EYFP) fusion protein driven by the *Camk2a* promoter[26] and observed intense ChR2-EYFP expression[27] in TC relay nuclei (**Fig. 4a**) and their projections in nRT (**Fig. 4b**) 4–8 weeks later. Fluorescence resulting from EYFP expression in TC neurons was seen during recordings in live slices as well as in fixed sections (**Fig. 4a**). High-magnification confocal images revealed that only TC neurons expressed the virus. Light stimulation of ChR2-expressing TC neurons evoked direct depolarizations with short latencies (data not shown).

To examine the properties of EPSCs evoked in nRT by selective optical stimulation of presumably one TC axon (**Fig. 4c**), we used a minimal stimulation protocol (see Online Methods). Minimally evoked EPSCs (eEPSCs) were similar in wild-type and *Gria4*$^{-/-}$ mice (**Fig. 4d**). We analyzed the mean eEPSC response from multiple nRT neurons from three wild-type ($n = 14$ cells) and three *Gria4*$^{-/-}$ ($n = 9$ cells) mice. The amplitude of minimal eEPSCs was similar in wild-type and *Gria4*$^{-/-}$ mice (wild type, 99.8 ± 20.4 pA; *Gria4*$^{-/-}$, 89.5 ± 9.93 pA; $P > 0.7$). In both genotypes, eEPSCs were characterized by fast activation kinetics (10–90% rise-time: wild type, 0.29 ± 0.01 ms; *Gria4*$^{-/-}$, 0.29 ± 0.02 ms; $P > 0.8$) and fast decay kinetics ($\tau_{D,W}$: wild type, 0.74 ± 0.05 ms; *Gria4*$^{-/-}$, 0.72 ± 0.09 ms; $P > 0.8$). We extended the analysis beyond mean values and found that these results were also reflected in cumulative probabilities that represent heterogeneity of events (**Fig. 4e**). Moreover, the input-output relationships of eEPSCs were not affected in the TC-nRT pathway (**Supplementary Fig. 2**). These findings indicate that the TC-nRT pathway is not affected by the absence of GluA4.

GluA4 deficiency reduces EPSCs at CT-nRT synapses

We next asked whether the absence of GluA4 altered synaptic excitation in the CT-nRT pathway. For this purpose, we injected ChR2-EYFP virus into deep layers of somatosensory cortex, which project to thalamus[28,29]. EYFP labeling in the cortex, as assessed from coronal cortical sections, was found throughout deep cortical layers (**Fig. 5a**) at the injection site. In the same hemisphere, EYFP labeling was found in horizontal thalamic sections in CT axons in nRT (**Fig. 5b**). Fluorescence resulting from EYFP expression in CT axons was seen during recordings in live

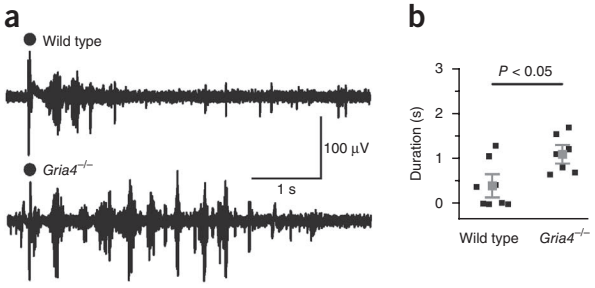

Figure 2 Evoked oscillations are enhanced in thalamic slices from *Gria4*$^{-/-}$ mice. (**a**) Multiunit recordings of intra-thalamic oscillations from wild-type and *Gria4*$^{-/-}$ thalamic slices evoked by single electrical shocks applied to internal capsule. Black dots indicate stimulation artifacts. (**b**) Averaged durations of the evoked oscillations were significantly increased in *Gria4*$^{-/-}$ mice compared with wild-type mice ($P < 0.05$, Mann-Whitney test). Gray squares indicate the population average, black squares indicate average response durations from individual slices calculated from 20 consecutive trials. Error bars represent s.e.m. We performed these recordings without any synaptic blockers (see Online Methods).

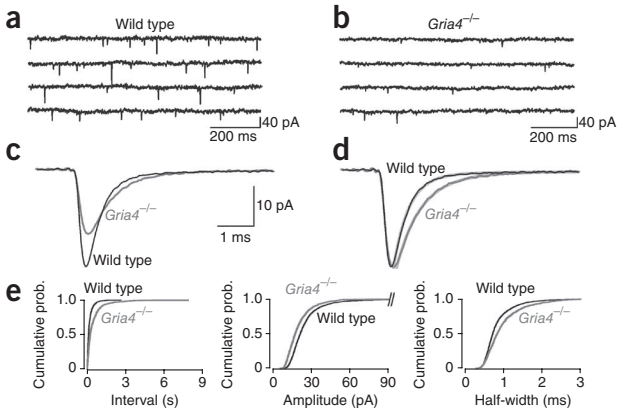

f

	Freq. (Hz)	Amplitude (pA)	Charge (fC)	$\tau_{D,W}$ (ms)	Rise time (ms)	Number of cells
Wild type	7.03 ± 0.85	24.3 ± 0.6	25.6 ± 0.9	0.76 ± 0.04	0.19 ± 0.01	20
Gria4$^{-/-}$	3.26 ± 0.57	20.0 ± 1.0	24.5 ± 0.9	1.60 ± 0.46	0.22 ± 0.01	16
ANOVA	$P < 0.05$	$P < 0.001$	$P > 0.4$	$P < 0.05$	$P > 0.08$	

Figure 3 Absence of AMPA receptor GluA4 alters synaptic excitation in thalamic reticular nucleus. (**a**,**b**) Spontaneous EPSC recordings from representative nRT neurons from wild-type (**a**) and *Gria4*$^{-/-}$ (**b**) mice. (**c**) Ensemble-averaged EPSCs from single nRT cells from wild-type (black) and *Gria4*$^{-/-}$ (dark gray) mice, plotted on the same timescale. (**d**) Normalized EPSCs depicted in **c**. Decay kinetics in *Gria4*$^{-/-}$ sEPSCs were slower than in wild type (light gray). (**e**) Cumulative probability histograms of isolated events from wild-type mice ($n = 20$ cells, 4,000 events, 200 events per cell) and *Gria4*$^{-/-}$ mice ($n = 16$ cells, 1,600 events, 100 events per cell) demonstrate differences in frequency, amplitude and kinetics ($P < 10^{-4}$, Kolmogoroff-Smirnoff test). (**f**) Quantification of the mean frequency, amplitude, charge, bi-exponential weighted decay-time constant ($\tau_{D,W}$) and 10–90% rise time of sEPSCs from 20 wild-type and 16 *Gria4*$^{-/-}$ nRT neurons. Statistical significance was determined by one-way ANOVA test. Error bars represent s.e.m. $\tau_{D,W}$ was calculated from the bi-exponential fits depicted in light gray in **d**.

slices as well as in fixed sections. High-magnification confocal images revealed that virus expression was specific to CT somata and axons; nRT neurons did not express the virus (**Fig. 5b**).

To examine the properties of EPSCs evoked in nRT by selective optical stimulation of CT axons (**Fig. 5c**), we used a minimal stimulation protocol. Resulting minimal eEPSCs were reduced in *Gria4*$^{-/-}$ versus wild-type mice (**Fig. 5d**). The mean eEPSC response was analyzed from multiple nRT neurons from three wild-type ($n = 9$ cells) and four *Gria4*$^{-/-}$ ($n = 6$ cells) mice. Notably, eEPSCs had slower decay kinetics and reduced amplitude in *Gria4*$^{-/-}$ mice ($\tau_{D,W}$: wild type, 1.33 ± 0.21 ms; *Gria4*$^{-/-}$, 1.59 ± 0.28 ms; amplitude: wild type, 43.5 ± 4.41 pA; *Gria4*$^{-/-}$, 29.3 ± 3.78 pA; $P < 0.05$; **Fig. 5d**,**e**). Synaptic efficacy, measured by the charge of eEPSCs, was also reduced in *Gria4*$^{-/-}$ mice (wild type, 72 ± 3.6 fC; *Gria4*$^{-/-}$, 53 ± 3.5 fC; $P < 0.01$), indicating that longer decay kinetics did not compensate for the reduced amplitude. Moreover, input-output relationships for eEPSCs were reduced in the CT-nRT pathway (**Supplementary Fig. 2**). These findings suggest that the CT-nRT excitatory pathway is weakened in the absence of GluA4.

GluA4 deficiency does not affect EPSCs at CT-TC synapses

In VB thalamus, clusters of EYFP-expressing CT axons were located in barreloids, as revealed by cytochrome C staining from the same slices (**Fig. 6a**). High-magnification confocal images revealed that virus expression was specific to CT somata and axons; TC neurons did not express the virus (**Fig. 6b**).

We examined whether the absence of GluA4 weakens the CT-TC pathway as it did the CT-nRT pathway. For this purpose, we examined CT-TC transmission by optical stimulation of CT axons (**Fig. 6c**) from the same wild-type and *Gria4*$^{-/-}$ mice slice preparations as we used to study the CT-nRT pathway.

Minimal eEPSCs were similar in wild-type and *Gria4*$^{-/-}$ mice (**Fig. 6d**,**e**). We analyzed the mean eEPSC response from multiple VB TC neurons from wild-type ($n = 5$) and *Gria4*$^{-/-}$ ($n = 5$) mice. The amplitude of minimal eEPSCs was similar in wild-type and *Gria4*$^{-/-}$ mice (wild type, 22.3 ± 0.83 pA; *Gria4*$^{-/-}$, 22.3 ± 1.8 pA; $P > 0.9$). In both genotypes, eEPSCs were characterized by similar activation kinetics (10–90% rise-time: wild type, 0.95 ± 0.26 ms; *Gria4*$^{-/-}$, 0.80 ± 0.16 ms; $P > 0.6$), decay kinetics ($\tau_{D,W}$: wild type, 3.7 ± 1.11 ms; *Gria4*$^{-/-}$, 3.9 ± 0.7 ms; $P > 0.8$) and half-width (wild type, 1.4 ± 0.2 ms; *Gria4*$^{-/-}$, 1.4 ± 0.3 ms; $P > 0.8$). These findings suggest that the CT-TC pathway is not affected in absence of GluA4. Notably, in the same slices, CT-nRT synaptic strength was weakened, whereas the CT-TC pathway was unaffected in *Gria4*$^{-/-}$ mice, suggesting that the altered response in nRT did not result from reduced optical activation from potential differences in viral expression between *Gria4*$^{-/-}$ and wild-type mice.

CT-nRT versus TC-nRT pathways

In both wild-type and *Gria4*$^{-/-}$ mice, cortically evoked EPSCs in nRT were smaller in amplitude and slower in rise and decay kinetics than TC-evoked responses (**Supplementary Fig. 3**). In wild-type mice, minimal EPSCs evoked by selective activation of CT axons were characterized by

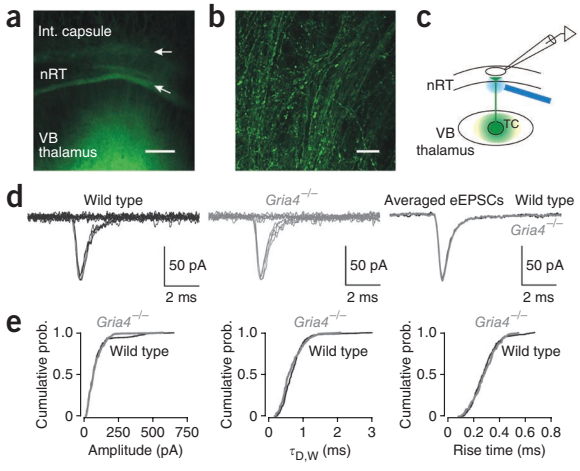

Figure 4 Selective optical stimulation of TC axons evokes similar EPSCs in nRT neurons from wild-type and *Gria4*$^{-/-}$ mice. (**a**) Low-magnification fluorescence image of a horizontal thalamic slice 6 weeks following intra-VB virus injection. The image was taken following fixation after electrophysiological recordings from the same slice. The EYFP signal was intense in VB and in the external medullary lamina (lower arrow) separating VB from nRT. The upper arrow indicates the border between nRT and the internal (int.) capsule. Scale bar represents 200 µm. (**b**) High-magnification confocal image from the same slice showing ChR2-expressing TC fibers in nRT. This image was obtained by a projection of *Z* stacks of confocal images acquired with a 0.5-µm optical step distance. Scale bar represents 20 µm. (**c**) Experimental configuration showing the locations of virus injection (VB, green spot), recording electrode (in nRT) and laser stimulation (blue beam). Stimuli were directed at ChR2-expressing TC axons and the eEPSC was recorded from an nRT cell. (**d**) Minimal EPSCs (50% of failures and 50% of eEPSCs) from single nRT neurons evoked by light activation of a TC axon from wild-type and *Gria4*$^{-/-}$ mice. Right, superimposition of averaged eEPSCs from the same cells. (**e**) Cumulative probability histograms of isolated events from wild-type mice (280 events from 14 nRT cells, 20 events per cell) and *Gria4*$^{-/-}$ mice (180 events from 9 nRT cells, 20 events per cell) demonstrate no changes in amplitude ($P > 0.8$), $\tau_{D,W}$ ($P > 0.1$) and 10–90% rise time ($P > 0.2$). Statistical significance in **e** was determined by the Kolmogoroff-Smirnoff test.

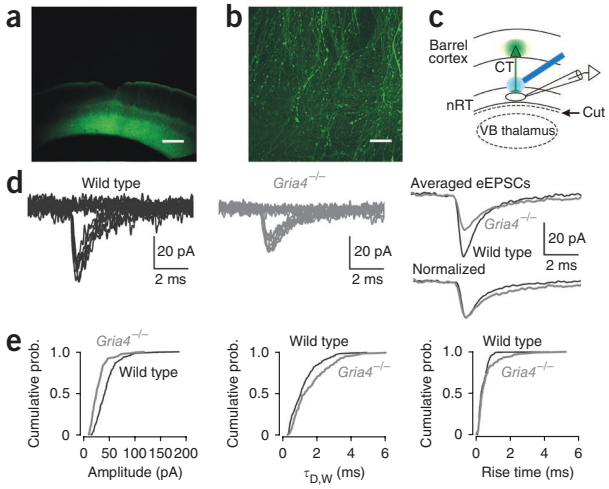

Figure 5 Selective optical stimulation of CT axons evokes smaller EPSCs in nRT neurons from *Gria4*$^{-/-}$ mice. (**a**) Low-magnification fluorescence image of a coronal slice from the barrel cortex 6 weeks following the intra-cortical virus injection. Fluorescence indicates ChR2 expression in the deep cortical layers (5/6). Scale bar represents 400 µm. (**b**) Higher magnification of a confocal image stack projection from a horizontal thalamic slice showing ChR2-expressing CT fibers in nRT. Scale bar represents 20 µm. (**c**) Experimental configuration showing locations of virus injection (cortex, green spot), recording electrode (in nRT) and laser stimulation (blue beam). Stimuli were directed at ChR2-expressing CT axons and the eEPSC was recorded from an nRT cell. VB thalamus was cut from the slices (dashed line) to avoid a disynaptic activation of nRT cells via the CT-TC-nRT pathway. (**d**) Minimal EPSCs (50% of failures and 50% of eEPSCs) in single nRT neurons evoked by light activation of a CT axon from wild-type and *Gria4*$^{-/-}$ mice. Top right, averaged eEPSCs from the corresponding nRT cells plotted on the same scale. Bottom right, normalized eEPSCs showing slower decay kinetics in *Gria4*$^{-/-}$ mice ($\tau_{D,W}$ = 1.89 ms) than in wild-type mice ($\tau_{D,W}$ = 1.18 ms). (**e**) Cumulative probability histograms of isolated events from wild-type mice (180 events from 9 nRT cells, 20 events per cell) and *Gria4*$^{-/-}$ mice (120 events from 6 nRT cells, 20 events per cell) show a reduction in amplitude ($P < 10^{-10}$), an increase in $\tau_{D,W}$ ($P < 0.01$) and no change in 10–90% rise time ($P > 0.1$). Statistical significance in **e** was determined by the Kolmogoroff-Smirnoff test.

an amplitude that was 2.3-fold smaller than that evoked by TC activation (CT-nRT, 43.5 ± 4.4 pA, $n = 9$ cells; TC-nRT, 99.8 ± 20.4 pA, $n = 14$ cells; $P < 0.003$) and were 1.8-fold slower ($\tau_{D,W}$: CT-nRT, 1.32 ± 0.21 ms, $n = 9$ cells; TC-nRT, 0.74 ± 0.05 ms, $n = 14$ cells; $P < 0.05$). In *Gria4*$^{-/-}$ mice, minimal EPSCs evoked by selective activation of CT axons were also characterized by an amplitude that was 3.1-fold smaller amplitude than that evoked by TC activation (CT-nRT, 29.3 ± 3.78 pA, $n = 6$ cells; TC-nRT, 89.5 ± 9.93 pA, $n = 9$ cells; $P < 0.003$) and 2.2-fold slower ($\tau_{D,W}$: CT-nRT, 1.59 ± 0.28 ms; TC-nRT, 0.72 ± 0.09 ms; $P < 0.004$).

Notably, the relative difference between CT- and TC-evoked EPSCs in nRT neurons was increased in *Gria4*$^{-/-}$ mice (TC-nRT:CT-nRT, ~3:1) compared with wild-type mice (TC-nRT:CT-nRT, ~2:1), which was a result of a weakened CT-nRT pathway and an unchanged TC-nRT pathway in the *Gria4*$^{-/-}$ mice (**Supplementary Fig. 3**). These results indicate that there is an enhanced imbalance between CT-nRT and TC-nRT pathways in the *Gria4*$^{-/-}$ mice, favoring TC versus CT synaptic inputs onto nRT neurons.

Synaptic integration in TC-nRT, CT-nRT and CT-TC pathways

We next asked whether synaptic integrative properties were also specifically reduced at CT-nRT synapses, leaving CT-TC and TC-nRT synapses unaffected. Thalamic neurons are capable of firing high-frequency bursts of action potentials both *in vivo*, during physiological spindle-wave activity and pathological SWDs[30–32], and *in vitro*[33,34]. High-frequency firing in TC neurons leads to high-frequency bursts of excitatory postsynaptic potentials (EPSPs) in the target nRT neurons[34]. We examined whether this integrative property was altered in absence of GluA4 in the TC-nRT pathway by optically stimulating ChR2-expressing TC fibers at a high frequency and comparing the evoked firing properties in target nRT cells from wild-type and *Gria4*$^{-/-}$ mice. Minimally stimulating (minimal intensity determined during voltage-clamp recordings as described for **Fig. 4c–e**) TC fibers drove similar action potential firing in nRT cells from both wild-type and *Gria4*$^{-/-}$ mice (**Fig. 7a**). This result indicates that integrative properties in the TC-nRT pathway are not affected in absence of GluA4 and suggests that activation of one TC fiber can drive robust firing in nRT cells.

We next examined whether evoked firing in the CT-nRT pathway was reduced in *Gria4*$^{-/-}$ mice. VB thalamus was cut from the slices (**Fig. 5c**) to avoid disynaptic activation of nRT cells via the CT-TC-nRT pathway. This procedure did not affect the electrical membrane properties of nRT neurons (**Supplementary Table 1**). Minimally stimulating (minimal

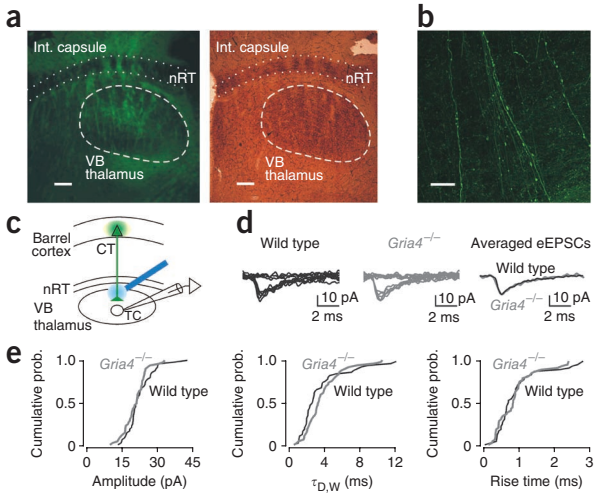

Figure 6 Selective optical stimulation of CT axons evokes similar EPSCs in TC neurons from wild-type and *Gria4*$^{-/-}$ mice. (**a**) Left, low-magnification fluorescence image of a horizontal thalamic slice 6 weeks after the virus injection in the barrel cortex. The image was taken following fixation after electrophysiological recordings of TC cells from the same slice. Fluorescent bundles corresponding to ChR2-expressing CT axonal terminals were observed in VB (dashed circle). Scale bar represents 200 µm. Right, cytochrome C staining from the same slice illustrating barreloids (dashed circle). (**b**) High-magnification confocal image stack projection from a horizontal thalamic slice showing ChR2-expressing CT fibers in VB thalamus. Scale bar represents 20 µm. (**c**) Experimental configuration showing the locations of virus injection (cortex, green spot), recording electrode (in VB) and laser stimulation (blue beam). Stimuli were directed at ChR2-expressing CT axons and the eEPSCs were recorded from a TC cell. (**d**) Minimal EPSCs (50% of failures and 50% of eEPSCs) in single TC neurons evoked by light activation of a CT axon from wild-type and *Gria4*$^{-/-}$ mice. Right, averaged eEPSCs from the same TC cells plotted on the same scale. (**e**) Cumulative probability histograms of isolated events from wild-type mice (50 events from 5 TC cells, 10 events per cell) and *Gria4*$^{-/-}$ mice (50 events from 5 TC cells, 10 events per cell) demonstrate no changes in amplitude ($P > 0.3$), $\tau_{D,W}$ ($P > 0.05$) and 10–90% rise time ($P > 0.5$). Statistical significance in **e** was determined by the Kolmogoroff-Smirnoff test.

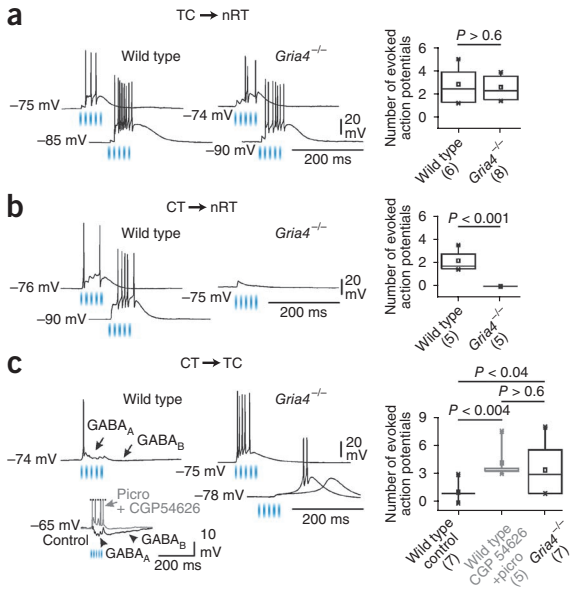

Figure 7 Specific reduction in the synaptic strength of the CT-nRT pathway in *Gria4*$^{-/-}$ mice abolishes the feed-forward inhibition in the CT-nRT-TC pathway and results in a hyperactivation of TC cells by CT inputs. (**a**) Optical stimulation (70 Hz, $n = 5$ light pulses, threshold intensity) of TC fibers evoked a similar firing rate in nRT neurons from wild-type and *Gria4*$^{-/-}$ mice. (**b**) Optical stimulation (70 Hz, $n = 5$ light pulses, 1.5× threshold intensity) of CT fibers evoked firing in nRT neurons from wild-type mice, but not from *Gria4*$^{-/-}$ mice. (**c**) Optical stimulation (70 Hz, $n = 5$ light pulses, 1.5× threshold intensity) of CT fibers evoked an immediate or late robust firing of action potentials in two different *Gria4*$^{-/-}$ TC cells. In wild-type TC neurons, CT stimulation evoked only one action potential that was interrupted by a burst of inhibitory postsynaptic potentials, followed by a long-lasting (~200 ms) hyperpolarization. Inset (bottom traces), superimposition of evoked responses from the same wild-type TC cell before (black) and after application of antagonists of $GABA_A$ and $GABA_B$ receptors (50 μM picrotoxin (picro) and 60 nM CGP54626, respectively; gray). Note that blocking $GABA_A$ and $GABA_B$ receptors in wild-type TC cells phenocopied the enhanced evoked firing from *Gria4*$^{-/-}$ TC cells. The horizontal dashed line indicates truncated action potentials. The number of action potentials reported in the statistical plots was assessed at resting membrane potential. The number of cells is indicated in parentheses. Statistical box charts show the mean (central dot), median (large horizontal line), maximal and minimal values (short horizontal lines), 99% and 1% range (crosses), 25–75% percentile range (box), and 5–95% percentile range (whiskers). Statistical significance was determined by one-way ANOVA test.

intensity determined as described for **Fig. 5**) ChR2-expressing CT fibers did not induce firing in nRT cells from wild-type mice (data not shown), suggesting that activation of one CT fiber is insufficient to drive firing in nRT. We found that 1.5× threshold intensity of high-frequency optical stimulation of CT fibers was necessary to evoke firing in nRT neurons from wild-type mice (**Fig. 7b**). In contrast, in *Gria4*$^{-/-}$ mice, CT fiber stimulation systematically failed to induce firing (**Fig. 7b**), even at 5× threshold stimulation intensities (data not shown). The absence of evoked firing in nRT cells was not a result of a reduced intrinsic excitability of these cells, which was similar in wild-type and *Gria4*$^{-/-}$ mice (**Supplementary Table 1**). The inability of CT fibers to drive nRT cell firing is consistent with the reduced eEPSC amplitudes in the CT-nRT pathway (**Fig. 5** and **Supplementary Fig. 2**).

Finally, we examined whether integrative properties of the CT-TC pathway were affected in the absence of GluA4 by optically stimulating ChR2-expressing CT fibers at a high frequency and comparing the evoked firing properties in TC cells from wild-type and *Gria4*$^{-/-}$ mice. In wild-type mice, 1.5× threshold intensity (threshold determined as explained in **Fig. 6**) was required to evoke an action potential in TC cells (**Fig. 7c**), and higher stimulation intensities failed to induce stronger firing in six of seven cells (data not shown). CT fiber stimulation evoked at most one action potential and a burst of high-frequency inhibitory postsynaptic potentials followed by a long-lasting (~200 ms) hyperpolarization (**Fig. 7c**). Early/fast and late/slow hyperpolarizations were abolished by blocking $GABA_A$ and $GABA_B$ receptors, suggesting that, in wild-type mice, CT inputs were not able to strongly drive TC cell firing because of a robust shunting inhibition of these cells. In *Gria4*$^{-/-}$ mice, CT fiber stimulation induced a robust and long-lasting burst firing in TC cells (1–8 action potentials; **Fig. 7c**). Notably, intrinsic membrane properties of TC neurons were similar in wild-type and *Gria4*$^{-/-}$ mice (**Supplementary Fig. 4a–c**). Moreover, inhibitory postsynaptic currents (IPSCs) evoked in TC neurons by stimulation of nRT axons were similar in wild-type and *Gria4*$^{-/-}$ mice (**Supplementary Fig. 4d**). Thus, the enhanced firing in TC neurons evoked by stimulation of CT axons was not a result of changes in intrinsic excitability of TC cells and/or from a reduction in nRT-TC synaptic strength in *Gria4*$^{-/-}$ mice.

We next examined the cellular and synaptic mechanisms (**Supplementary Fig. 5**) underlying the circuit hyperexcitability using similar conditions as those used to assess network oscillations (**Fig. 2**). We examined the effects of traditional electrical stimulation of the internal capsule (containing both CT and TC fibers) on the firing of nRT and TC cells. In contrast with optical stimulations, we used the minimal firing protocol (leading to ~50% of responses that were suprathreshold for action potential generation intermixed with action potential failures). Similar to optical stimulations, high-frequency electrical stimulations led to robust and long-lasting firing in TC neurons from *Gria4*$^{-/-}$ mice and only single action potentials in wild-type mice (**Supplementary Fig. 5a**,**b**,**f**,**h**). In wild-type mice, CT-nRT-TC feed-forward inhibition includes a late component that is mediated by $GABA_B$ receptors[33,35,36], which was not blocked in these experimental conditions. Notably, this prolonged firing in TC cells was followed by a late and enhanced nRT cell firing in *Gria4*$^{-/-}$ mice (1–12 action potentials) that was not observed in wild-type mice (**Supplementary Fig. 5c**,**d**). Thus, the threshold electrical stimulation, which was similar in both genotypes (wild type, 24.6 ± 1.89 V, $n = 31$ cells; *Gria4*$^{-/-}$, 27.5 ± 3.27 V, $n = 18$ cells; $P > 0.4$), induced an overall higher firing rate in nRT neurons from *Gria4*$^{-/-}$ than in those from wild-type mice (**Supplementary Fig. 5c**,**d**). Notably, passive and active intrinsic electrical membrane properties in both TC and nRT neurons were similar between wild-type and *Gria4*$^{-/-}$ mice (**Supplementary Fig. 4a–c** and **Supplementary Table 1**). Thus, the more robust and prolonged evoked firing in TC and nRT neurons in *Gria4*$^{-/-}$ cannot be accounted for by a change in intrinsic membrane excitability. Differences in optically or electrically evoked firing between *Gria4*$^{-/-}$ and wild-type mice were not dependent on membrane potential (between –55 mV and –90 mV, data not shown), indicating that they were independent of firing mode (that is, burst versus regular).

DISCUSSION

Although there is some controversy regarding the role of the thalamus in seizure initiation, it is regarded as an important rhythm generator in the thalamocortical network[3,7,10,34]. We found that GluA4 deficiency specifically and selectively reduced the strength of CT-nRT, but not TC-nRT, synapses, which is surprising given the prominent expression of GluA4 receptors in nRT. GluA4 deficiency did not affect the fastest EPSCs in nRT (that is, TC-nRT EPSCs), suggesting that GluA4 is not strictly required for fast kinetics. This is surprising to us, as the AMPA receptor subunit GluA4 is thought to show the fastest kinetics[37,38] and its loss would be expected to prolong the TC-nRT EPSCs in nRT.

Specific weakening of CT-nRT synapses led to a loss of CT-nRT-TC feed-forward inhibition, which resulted in increased CT-TC excitability and the initiation of synchronous network oscillation in thalamus via the CT-TC-nRT channel. Finally, retention of TC-nRT excitation and of nRT-TC feedback inhibition in *Gria4*$^{-/-}$ mice allowed the maintenance of thalamic oscillations.

GluA4 deficiency specifically weakens CT-nRT synapses

In the absence of GluA4, sEPSCs in nRT neurons were reduced in amplitude (~18%) and showed twofold slower decay. AMPA receptors are tetrameric assemblies of subunits GluA1–4 and are generally heteromeric. GluA4 is expressed in a small number of neocortical neurons, but is mostly expressed in the thalamus, particularly in nRT, where it is the predominant AMPA receptor subunit at the CT-nRT synapse, with 3.7-fold higher expression on nRT than on TC neurons[11,13,39]. GluA4-containing receptors have the fastest desensitization rate[37,38] compared with other subunits expressed in the nRT[11,12,20]. Thus, the loss of the GluA4 subunit is consistent with the reduced amplitude and the slower decay kinetics of sEPSCs in nRT neurons. These results are consistent with previous findings showing similar changes in sEPSC amplitude and kinetics in mice with a hypomorphic mutation in the *Gria4* gene that was associated with a reduced expression of GluA4 protein[20]. Furthermore, we found that, in the absence of GluA4, minimal EPSCs evoked by optical stimulation of putative single CT axons were also smaller in amplitude and slower in decay kinetics. Altogether, these results indicate that GluA4 is crucial for spontaneous and evoked CT-nRT transmission. Notably, minimal EPSCs evoked by optical stimulation of single TC axons were not affected by GluA4 deficiency. Our finding that the absence of GluA4 did not affect TC-nRT synaptic strength suggests that GluA4 has a minor role in TC-nRT synaptic transmission. In addition, our results suggest that the reduced frequency of sEPSCs in nRT neurons from *Gria4*$^{-/-}$ mice largely reflect a reduced strength in CT-nRT synapses, which are the most numerous excitatory synapses in nRT[40,41].

In contrast with nRT neurons, GluA4 deficiency did not affect sEPSCs or cortically evoked EPSCs in TC neurons. This suggests that GluA4 receptor have less involvement in CT-TC transmission than in CT-nRT transmission. This is consistent with the finding that there is a ~fourfold weaker expression of GluA4 at CT synapses in TC neurons compared with nRT neurons[13]. A weak expression of GluA4 in TC neurons is consistent with a smaller amplitude of sEPSCs and eEPSCs in TC versus nRT neurons, 3.3-fold slower decay kinetics of sEPSCs in TC neurons compared with nRT neurons, and 2.8-fold slower decay kinetics of minimal EPSCs evoked by optical stimulation of single CT axons compared with those evoked in nRT. The fact that GluA4 deficiency does not affect excitatory currents in TC neurons could also be a result of a compensatory increase in expression of other AMPA receptor subunits, such as GluA3 and, to a lesser degree, GluA2, which are also expressed in the thalamus[13]. The slower rise and decay kinetics of sEPSCs and eEPSCs in TC neurons compared with nRT neurons could also be a result of the fact that CT synapses on TC neurons are concentrated on distal dendrites[42,43]. Discrepancies between our results and those of a previous study[13], which found similar EPSC kinetics in nRT and TC cells, could result from differences in the maturation state of mice that were used.

Why are nRT EPSCs evoked by TC activation faster than those evoked by CT activation? It is important to emphasize that the rise times and decay-time constants of minimal EPSCs evoked in nRT neurons by CT optical activation were much slower than those evoked by TC optical activation. This suggests that TC-nRT eEPSCs originated from electrotonically closer synaptic terminals on the dendrites than did CT-nRT eEPSCs[40,41], rather than resulting from a stronger expression of GluA4 on TC-nRT synapses, as GluA4 deficiency had no effect on eEPSC kinetics in TC-nRT synapses.

Altogether, our results indicate that GluA4 deficiency specifically reduced CT-nRT synaptic strength without affecting CT-TC and TC-nRT synaptic strengths. Thus, the reduced excitation of nRT neurons in *Gria4*$^{-/-}$ mice results from a specific defect in CT synapses on nRT cells, which represent the main excitatory input onto nRT[40,41].

Mechanisms of thalamic hyperexcitability in *Gria4*$^{-/-}$ mice

Gria4$^{-/-}$ mice display absence epileptic seizures and thalamic circuit hyperexcitability. Even though GluA4 expression is minor in the cerebral cortex compared with the thalamus[12], we cannot exclude the notion that absence seizures could partially result from alterations in excitatory synaptic transmission in the cortex, presumably to a minor degree compared with thalamus. However, given that isolated thalamic slices are hyperexcitable and that synaptic strength is specifically reduced in CT-nRT pathway, we propose that hyperexcitability in the cortico-thalamo-cortical system ultimately results from a specific defect in CT-nRT synapses.

The increased excitability in thalamic networks is surprising because one would expect thalamic hypersynchronicity to be associated with an increased excitation (for example, in the TC-nRT pathway) rather than with a reduced excitatory strength. How does a reduced synaptic strength in the CT-nRT pathway lead to thalamic hyperexcitability and absence seizures? To address this question, we closely examined the cellular and synaptic mechanisms underlying the circuit hyperexcitability. Using optogenetics, we found that, in wild-type mice, CT inputs powerfully drive nRT cell firing, shunting direct CT-TC excitation. In *Gria4*$^{-/-}$ mice, the inability of CT inputs to drive nRT cell firing results in an inability of CT-nRT pathway to shunt the direct CT-TC excitation and allows CT inputs to robustly activate TC cells, thereby initiating an aberrant network oscillation. The oscillation is then maintained because the TC-nRT-TC circuit is intact.

In summary, we propose the following scenario of events leading to the initiation and maintenance of synchronous network oscillations. First, given the likely role of cortical output in the early stages of SWDs[44,45], activation of CT neurons leads to direct and prolonged activation of TC neurons, as CT-nRT-TC feed-forward inhibition is reduced and the CT-TC pathway is unaffected. Second, this direct hyperactivation of TC cells by CT inputs is sufficient to hyperactivate nRT neurons, as the synaptic strength of the TC-nRT pathway is normally quite strong[46] and is not weakened in the *Gria4*$^{-/-}$ mice. Third, nRT neurons fire high-frequency bursts of action potentials and inhibit TC neurons, which fire bursts of action potentials on recovery from inhibition. This sequence of events continues, leading to a robust oscillatory network in the cortico-thalamo-cortical loop[3,35,36] that promotes SWD seizures (see also **Supplementary Fig. 6**). In light of the controversy regarding the potential roles of cortex and thalamus in SWD initiation[44,45], we propose that, in *Gria4*$^{-/-}$ mice, SWDs can initiate as a result of an abnormal 'channel' of synaptic transmission between cortex and thalamus. This mode of communication in *Gria4*$^{-/-}$, but not wild-type, mice could allow intense, but physiologically relevant cortical activity to trigger epileptic thalamocortical network activity and lead to a transition between normal circuit function and epileptic seizure.

Our results describe a previously unknown circuit mechanism leading to absence epilepsy: a weakening of a single component of the CT excitatory pathway, the CT-nRT synapse. This ultimately leads to enhanced network synchrony from specific loss of feed-forward (CT-nRT-TC), but not feedback (TC-nRT-TC), inhibition. Our findings provide a new concept for the initiation of network oscillations that may apply to a variety of contexts; reduction of feed-forward inhibition enables afferent

excitatory inputs to recruit a critical mass of excitatory neurons whose simultaneous activation is sufficient to initiate synchronized network activities. Furthermore, this mode of information flow between cortex and thalamus may represent a previously unknown mode of sensory information processing. Indeed, when the CT-TC-nRT-TC window is open via reduction in CT-nRT-TC feed-forward inhibition, cortical inputs from layer 6 would become 'drivers', similar to those from layer 5 (ref. 47), directly engaging sensory thalamic neurons. Future studies should be aimed at determining whether this mode would be adaptive or maladaptive in the context of sensory processing.

METHODS

Methods and any associated references are available in the online version of the paper at http://www.nature.com/natureneuroscience/.

Note: Supplementary information is available on the Nature Neuroscience website.

ACKNOWLEDGMENTS

We thank I. Parada for her expert histology technical support and A. Herbert and S. Jin for their help with animal husbandry. We also thank T. Davidson for insightful discussions on the optogenetic approach and C. Lee for a generous help during virus injections. This work was supported by grants from the US National Institutes of Health and the National Institute of Neurological Disorders and Stroke (NS34774, NS06477 and NS031348), the DARPA REPAIR program and the Epilepsy Foundation.

AUTHOR CONTRIBUTIONS

J.T.P. and J.R.H. designed the experiments and wrote the manuscript. L.F., O.Y., K.D. and W.N.F. provided reagents and tools. J.T.P., A.S.B. and K.P. carried out the experiments. J.T.P., A.S.B., K.P. and J.R.H. analyzed the data.

COMPETING FINANCIAL INTERESTS

The authors declare no competing financial interests.

Published online at http://www.nature.com/natureneuroscience/.
Reprints and permissions information is available online at http://www.nature.com/reprints/index.html.

1. Steriade, M. Corticothalamic networks, oscillations, and plasticity. *Adv. Neurol.* **77**, 105–134 (1998).
2. Mountcastle, V. *Perceptual Neuroscience* (Harvard University Press, Cambridge, Massachusetts, 1998).
3. Beenhakker, M.P. & Huguenard, J.R. Neurons that fire together also conspire together: is normal sleep circuitry hijacked to generate epilepsy? *Neuron* **62**, 612–632 (2009).
4. Steriade, M. & Contreras, D. Relations between cortical and thalamic cellular events during transition from sleep patterns to paroxysmal activity. *J. Neurosci.* **15**, 623–642 (1995).
5. Sillito, A.M. & Jones, H.E. Corticothalamic interactions in the transfer of visual information. *Phil. Trans. R. Soc. Lond. B* **357**, 1739–1752 (2002).
6. von Krosigk, M., Monckton, J.E., Reiner, P.B. & McCormick, D.A. Dynamic properties of corticothalamic excitatory postsynaptic potentials and thalamic reticular inhibitory postsynaptic potentials in thalamocortical neurons of the guinea-pig dorsal lateral geniculate nucleus. *Neuroscience* **91**, 7–20 (1999).
7. Warren, R.A., Agmon, A. & Jones, E.G. Oscillatory synaptic interactions between ventroposterior and reticular neurons in mouse thalamus *in vitro*. *J. Neurophysiol.* **72**, 1993–2003 (1994).
8. Destexhe, A., Contreras, D. & Steriade, M. Mechanisms underlying the synchronizing action of corticothalamic feedback through inhibition of thalamic relay cells. *J. Neurophysiol.* **79**, 999–1016 (1998).
9. Pinault, D. *et al.* Intracellular recordings in thalamic neurones during spontaneous spike and wave discharges in rats with absence epilepsy. *J. Physiol. (Lond.)* **509**, 449–456 (1998).
10. von Krosigk, M., Bal, T. & McCormick, D.A. Cellular mechanisms of a synchronized oscillation in the thalamus. *Science* **261**, 361–364 (1993).
11. Keinänen, K. *et al.* A family of AMPA-selective glutamate receptors. *Science* **249**, 556–560 (1990).
12. Petralia, R.S. & Wenthold, R.J. Light and electron immunocytochemical localization of AMPA-selective glutamate receptors in the rat brain. *J. Comp. Neurol.* **318**, 329–354 (1992).
13. Golshani, P., Liu, X.B. & Jones, E.G. Differences in quantal amplitude reflect GluR4-subunit number at corticothalamic synapses on two populations of thalamic neurons. *Proc. Natl. Acad. Sci. USA* **98**, 4172–4177 (2001).
14. Nagel, G. *et al.* Channelrhodopsin-2, a directly light-gated cation-selective membrane channel. *Proc. Natl. Acad. Sci. USA* **100**, 13940–13945 (2003).
15. Boyden, E.S., Zhang, F., Bamberg, E., Nagel, G. & Deisseroth, K. Millisecond-timescale, genetically targeted optical control of neural activity. *Nat. Neurosci.* **8**, 1263–1268 (2005).
16. Cardin, J.A. *et al.* Driving fast-spiking cells induces gamma rhythm and controls sensory responses. *Nature* **459**, 663–667 (2009).
17. Petreanu, L., Huber, D., Sobczyk, A. & Svoboda, K. Channelrhodopsin-2-assisted circuit mapping of long-range callosal projections. *Nat. Neurosci.* **10**, 663–668 (2007).
18. Sohal, V.S., Zhang, F., Yizhar, O. & Deisseroth, K. Parvalbumin neurons and gamma rhythms enhance cortical circuit performance. *Nature* **459**, 698–702 (2009).
19. Cruikshank, S.J., Urabe, H., Nurmikko, A.V. & Connors, B.W. Pathway-specific feedforward circuits between thalamus and neocortex revealed by selective optical stimulation of axons. *Neuron* **65**, 230–245 (2010).
20. Beyer, B. *et al.* Absence seizures in C3H/HeJ and knockout mice caused by mutation of the AMPA receptor subunit Gria4. *Hum. Mol. Genet.* **17**, 1738–1749 (2008).
21. Bryant, A.S., Li, B., Beenhakker, M.P. & Huguenard, J.R. Maintenance of thalamic epileptiform activity depends on the astrocytic glutamate-glutamine cycle. *J. Neurophysiol.* **102**, 2880–2888 (2009).
22. Schofield, C.M., Kleiman-Weiner, M., Rudolph, U. & Huguenard, J.R. A gain in $GABA_A$ receptor synaptic strength in thalamus reduces oscillatory activity and absence seizures. *Proc. Natl. Acad. Sci. USA* **106**, 7630–7635 (2009).
23. Bernardo, K.L. & Woolsey, T.A. Axonal trajectories between mouse somatosensory thalamus and cortex. *J. Comp. Neurol.* **258**, 542–564 (1987).
24. Agmon, A., Yang, L.T., O'Dowd, D.K. & Jones, E.G. Organized growth of thalamocortical axons from the deep tier of terminations into layer IV of developing mouse barrel cortex. *J. Neurosci.* **13**, 5365–5382 (1993).
25. Pinault, D., Bourassa, J. & Deschênes, M. The axonal arborization of single thalamic reticular neurons in the somatosensory thalamus of the rat. *Eur. J. Neurosci.* **7**, 31–40 (1995).
26. Dittgen, T. *et al.* Lentivirus-based genetic manipulations of cortical neurons and their optical and electrophysiological monitoring *in vivo*. *Proc. Natl. Acad. Sci. USA* **101**, 18206–18211 (2004).
27. Lee, J.H. *et al.* Global and local fMRI signals driven by neurons defined optogenetically by type and wiring. *Nature* **465**, 788–792 (2010).
28. Bourassa, J., Pinault, D. & Deschênes, M. Corticothalamic projections from the cortical barrel field to the somatosensory thalamus in rats: a single-fibre study using biocytin as an anterograde tracer. *Eur. J. Neurosci.* **7**, 19–30 (1995).
29. Hoogland, P.V., Welker, E. & Van der Loos, H. Organization of the projections from barrel cortex to thalamus in mice studied with *Phaseolus vulgaris*-leucoagglutinin and HRP. *Exp. Brain Res.* **68**, 73–87 (1987).
30. Pinault, D. Cellular interactions in the rat somatosensory thalamocortical system during normal and epileptic 5–9 Hz oscillations. *J. Physiol. (Lond.)* **552**, 881–905 (2003).
31. Steriade, M. Sleep, epilepsy and thalamic reticular inhibitory neurons. *Trends Neurosci.* **28**, 317–324 (2005).
32. Paz, J.T., Chavez, M., Saillet, S., Deniau, J. & Charpier, S. Activity of ventral medial thalamic neurons during absence seizures and modulation of cortical paroxysms by the nigrothalamic pathway. *J. Neurosci.* **27**, 929–941 (2007).
33. Huguenard, J.R. & Prince, D.A. Intrathalamic rhythmicity studied *in vitro*: nominal T-current modulation causes robust antioscillatory effects. *J. Neurosci.* **14**, 5485–5502 (1994).
34. Bal, T., von Krosigk, M. & McCormick, D.A. Role of the ferret perigeniculate nucleus in the generation of synchronized oscillations *in vitro*. *J. Physiol. (Lond.)* **483**, 665–685 (1995).
35. Bal, T., Debay, D. & Destexhe, A. Cortical feedback controls the frequency and synchrony of oscillations in the visual thalamus. *J. Neurosci.* **20**, 7478–7488 (2000).
36. Blumenfeld, H. & McCormick, D.A. Corticothalamic inputs control the pattern of activity generated in thalamocortical networks. *J. Neurosci.* **20**, 5153–5162 (2000).
37. Mosbacher, J. *et al.* A molecular determinant for submillisecond desensitization in glutamate receptors. *Science* **266**, 1059–1062 (1994).
38. Geiger, J.R. *et al.* Relative abundance of subunit mRNAs determines gating and Ca^{2+} permeability of AMPA receptors in principal neurons and interneurons in rat CNS. *Neuron* **15**, 193–204 (1995).
39. Mineff, E.M. & Weinberg, R.J. Differential synaptic distribution of AMPA receptor subunits in the ventral posterior and reticular thalamic nuclei of the rat. *Neuroscience* **101**, 969–982 (2000).
40. Ohara, P.T. & Lieberman, A.R. The thalamic reticular nucleus of the adult rat: experimental anatomical studies. *J. Neurocytol.* **14**, 365–411 (1985).
41. Liu, X.B. & Jones, E.G. Predominance of corticothalamic synaptic inputs to thalamic reticular nucleus neurons in the rat. *J. Comp. Neurol.* **414**, 67–79 (1999).
42. Jones, E.G. & Powell, T.P. An electron microscopic study of the mode of termination of cortico-thalamic fibres within the sensory relay nuclei of the thalamus. *Proc. R. Soc. Lond. B Biol. Sci.* **172**, 173–185 (1969).
43. Liu, X.B., Warren, R.A. & Jones, E.G. Synaptic distribution of afferents from reticular nucleus in ventroposterior nucleus of cat thalamus. *J. Comp. Neurol.* **352**, 187–202 (1995).
44. Meeren, H.K.M., Pijn, J.P.M., Van Luijtelaar, E.L.J.M., Coenen, A.M.L. & Lopes da Silva, F.H. Cortical focus drives widespread corticothalamic networks during spontaneous absence seizures in rats. *J. Neurosci.* **22**, 1480–1495 (2002).
45. Polack, P.O. *et al.* Deep layer somatosensory cortical neurons initiate spike-and-wave discharges in a genetic model of absence seizures. *J. Neurosci.* **27**, 6590–6599 (2007).
46. Gentet, L.J. & Ulrich, D. Strong, reliable and precise synaptic connections between thalamic relay cells and neurones of the nucleus reticularis in juvenile rats. *J. Physiol. (Lond.)* **546**, 801–811 (2003).
47. Sherman, S.M. & Guillery, R.W. On the actions that one nerve cell can have on another: distinguishing "drivers" from "modulators". *Proc. Natl. Acad. Sci. USA* **95**, 7121–7126 (1998).

ONLINE METHODS

We performed all of the experiments according to protocols approved by the Stanford Institutional Animal Care and Use Committee, and every precaution was taken to minimize stress and the number of animals used in each series of experiments.

Mice. *Gria4* knockout mice (B6;129P2-*Gria4*^{tm1Dgen})[20], constructed by Deltagen and obtained from the Mouse Mutant Regional Resource Consortium repository, were backcrossed to the C57BL/6J strain for ten generations and then maintained as a homozygous colony. Wild-type mice were maintained separately on a C57BL/6J background. We refer to the B6;129P2-*Gria4*^{tm1Dgen} mice[20] as *Gria4*$^{-/-}$ mice.

EEG analysis. We anesthetized male mice at least 30 d postnatal using isoflurane inhalation at 1 l min^{-1} oxygen flow (3% isoflurane (vol/vol) flow for induction, 1–2% isoflurane flow for maintenance). We injected the pre-operative analgesic carprofen (5 mg per kg of body weight) intraperitoneally. We drilled four holes of approximately 0.6-mm diameter through the skull, each about 5 mm lateral from the sagittal suture and in line with lambda and bregma. A fifth hole was drilled in the interparietal bone, slightly lateral of midline for the ground electrode. We mounted a small plug (2-mm dual pin gull wing connector socket, Digi-Key) with attached stainless steel wires (Medwire 316 SS 7/44T) terminated with screws (2.38-mm-long #303SS, J.J. Morris). We secured the screws into the skull holes with 2–3 turns each, and stabilized the whole unit with dental cement. We performed EEG recordings after at least 7 d of postsurgery recovery. Mice were placed in a dedicated cage and attached to an XLTek 32 Channel EEG headbox via a 50-cm, 6 channel, plastic-encased cable. We collected simultaneous video and EEG recordings. We recorded spontaneous SWDs characteristic of absence seizures simultaneously with video monitoring for 60 min before ethosuximide (200 mg per kg, intraperitoneal) injection. We then recorded for, at minimum, an additional 1 h. The control mice were injected intraperitoneally with saline and recorded in the same manner. We band-pass filtered the recordings off-line and performed wavelet analysis with MatLab (MathWorks)[22].

Thalamic oscillations. We placed horizontal slices (400 μm) containing somatosensory thalamus in an interface chamber at 34 °C and superfused them at a rate of 2 ml min^{-1} with oxygenated artificial cerebrospinal fluid (ACSF) containing 126 mM NaCl, 2.5 mM KCl, 1.25 mM NaH_2PO_4, 2 mM $MgCl_2$, 2 mM $CaCl_2$, 26 mM $NaHCO_3$ and 10 mM glucose, equilibrated with 95% O_2 and 5% CO_2, pH 7.4, supplemented with 0.3 mM glutamine[21]. We obtained extracellular multi-unit field recordings with monopolar tungsten microelectrodes (50–100 kΩ, FHC) placed in VB thalamus and in nRT. We amplified the signals 10,000 times and band-pass filtered them between 100 Hz and 3 kHz. We delivered electrical stimuli to the internal capsule with a pair of tungsten microelectrodes (50–100 kΩ, FHC). The stimuli were 100 μs in duration, 50 V in amplitude, and delivered once every 30 s.

***In vitro* slice preparation.** We anesthetized and decapitated wild-type and *Gria4*$^{-/-}$ mice of either sex (postnatal day 18–120, P18–120) with pentobarbital (100 mg per kg, intraperitoneal). We rapidly removed the brains and immersed them in an ice-cold (4 °C) slicing solution containing 234 mM sucrose, 2.5 mM KCl, 1.25 mM NaH_2PO_4, 10 mM $MgSO_4$, 0.5 mM $CaCl_2$, 26 mM $NaHCO_3$ and 11 mM glucose, equilibrated with 95% O_2 and 5% CO_2, pH 7.4. We prepared 270-μm-thick horizontal thalamic slices containing VB thalamus and nRT with a Leica VT1200 microtome (Leica Microsystems). We incubated the slices, initially at 32 °C for 1 h and then at 24–26 °C, in ACSF containing 126 mM NaCl, 2.5 mM KCl, 1.25 mM NaH_2PO_4, 2 mM $MgCl_2$, 2 mM $CaCl_2$, 26 mM $NaHCO_3$ and 10 mM glucose, equilibrated with 95% O_2 and 5% CO_2, pH 7.4.

Electrophysiology. We made whole-cell patch-clamp recordings at 22–25 °C. Following incubation, we transferred brain slices to the recording chamber and superfused them with ACSF at a flow rate of 2 ml min^{-1}. We obtained recordings from nRT and TC neurons visually identified using differential contrast optics with a Zeiss (Oberkochen) Axioskop microscope and an infrared video camera. Recording electrodes made of borosilicate glass had a resistance of 2–5 MΩ when filled with intracellular solution. For IPSCs, the internal solution contained 135 mM CsCl, 10 mM HEPES, 10 mM EGTA, 5 mM QX-314 (lidocaine *N*-ethyl bromide) and 2 $MgCl_2$, pH adjusted to 7.3 with CsOH (290 mOsm). E_{Cl}^- was estimated to be ~0 mV based on the Nernst equation. During IPSC recordings, we clamped the neurons at −70 mV and recorded pharmacologically isolated events during bath application of the ionotropic glutamate receptor blockers DNQX (6,7-dinitroquinoxaline-2,3-dione, 20 μM, Ascent Scientific) and AP5 (2-amino-5-phosphonopentanoic acid, 100 μM, Ascent Scientific). For EPSCs and current-clamp recordings, the internal solution contained 120 mM potassium gluconate, 11 mM KCl, 1 mM $MgCl_2$, 1 mM $CaCl_2$, 10 mM HEPES, 1 mM EGTA, pH adjusted to 7.4 with KOH (290 mOsm). E_{Cl}^- was estimated to be about −60 mV based on the Nernst equation. Potentials were corrected for −15-mV liquid junction potential. During EPSC recordings, we clamped the neurons at −80 mV and recorded pharmacologically isolated AMPA currents by bath application of the $GABA_A$ receptor antagonist picrotoxin (50 μM, Tocris) and NMDA receptor antagonist (AP5, 100 μM). We blocked NMDA receptors to determine whether the differences in decay kinetics of spontaneous and evoked EPSCs in *Gria4*$^{-/-}$ versus wild-type mice resulted directly from a lack of GluA4 receptors rather than from long-lasting NMDA currents. In all recording conditions, we monitored access resistance, and cells were included for analysis only if the access resistance was <18 MΩ and the change of resistance was <25% over the course of the experiment. In addition, we demonstrated the adequacy of voltage clamp by T-current steady-state inactivation protocols in which peak latencies remained constant after voltage-clamp steps to −75 mV from a range of hyperpolarizing conditioning potentials as previously described[48]. We obtained evoked EPSPs and firing of nRT and VB TC cells with optical stimulations (see below) or with a concentric bipolar stimulating electrode positioned in striatum or internal capsule, activating both CT and TC fibers. Concerning electrical stimulations, we applied train stimuli (five pulses at 200 Hz) every 20 s. Antidromically activated TC neurons were not considered in the firing latency analysis (**Supplementary Fig. 5b**,**f**,**h**). We recorded EPSPs and firing evoked by optical stimulations (five pulses at 70 Hz; **Fig. 7a–c**) in the presence of 100 μM AP5 to ensure that differences in firing resulted from differences in AMPA receptors and not from secondary activation of NMDA receptors. In some experiments (**Fig. 7c**), we bath applied picrotoxin (50 μM) and CGP 54626 (60 nM, Tocris) to block $GABA_A$ and $GABA_B$ receptors, respectively. Given the properties of the opsin, it was not possible to use frequencies higher than 70 Hz (in contrast with electrical stimulations, performed at 200 Hz). However, 70-Hz stimulation was sufficient to drive burst firing in thalamic cells.

Optogenetics. We injected viruses carrying fusion genes for fluorescent proteins and ChR2 stereotaxically, generally bilaterally, into barrel cortex or VB thalamus of wild-type and *Gria4*$^{-/-}$ mice *in vivo*, between P22–35. Injection of viral DNA (rAAV5/CamKIIα-hChR2(H134R)-EYFP) under *Camk2a* promoter results in expression only in excitatory cortical and thalamic neurons[19]. We injected concentrated virus (2×10^{12} genome copies per milliliter) using a 10-μl syringe and 34-gauge needle; injected volume (900 nl for cortex and 600 nl for VB) and flow rate (100 nl min^{-1}) were controlled by pump (World Precision Instruments). For intra-cortical injections (wild type, $n = 6$ hemispheres from 3 mice; *Gria4*$^{-/-}$, $n = 7$ hemispheres from 4 mice), the stereotaxic coordinates were 1.3 mm posterior to Bregma, 3 mm lateral to the midline and 1.15 mm below the cortical surface. For intra-thalamic injections (wild-type, $n = 6$ hemispheres from 3 mice; *Gria4*$^{-/-}$, $n = 6$ hemispheres from 3 mice) the coordinates were 1.7 mm posterior to Bregma, 1.5 mm lateral and 3.5 mm below the cortical surface. We killed the mice 5–8 weeks following injections corresponding to P56–120 and acute horizontal brain thalamic slices were made for optical stimulations and *in vitro* recordings. We prepared thalamic slices and performed *in vitro* whole-cell recordings as described above. ChR2-expressing fibers were visualized with fluorescence microscopy. We optically activated ChR2-expressing CT and TC axons with blue laser stimuli (473 nm, 70 μW to 3 mW, 1–5 ms flashes; OEM Laser Systems) delivered with optic fiber (BFL 37–300, Thor Labs) upstream along the CT and TC pathways (see schematic diagrams in **Figs. 4c**, **5c** and **6c**). We used minimal stimulation intensity[49], defined as the light power that resulted in 50–70% failures (30–50% successes), fixed response kinetics and low response-amplitude variability. Consequent minimal eEPSCs presumably resulted from selective optical activation of single CT or TC axons presynaptic to the recorded cell. At the end of the recordings, we fixed the slices with 4% paraformaldehyde (wt/vol) solution, then resectioned at 80 μm and low- and obtained high-magnification images with fluorescence (Nikon) and confocal (Zeiss LSM 510) microscopes, respectively. In the intra-cortical virus injection experiments, we obtained both coronal cortical and

doi:10.1038/nn.2896

horizontal thalamic slices from the same mice and stained them for cytocrome C to confirm the virus injection site (barrel cortex) and to confirm the presence of ChR2-expressing CT axons and terminals in the VB barreloids (**Fig. 6a**)[50]. We recorded TC neurons from VB thalamus. Virus spread in somatosensory cortex and thalamus was reproducible across mice. Stimulation intensity and duration required for minimal eEPSCs were similar in *Gria4*$^{-/-}$ and wild-type mice, suggesting that virus expression was similar in both genotypes. Intrinsic electrical membrane properties were not affected in ChR2-expressing TC neurons or in their target nRT neurons (data not shown), and were not affected in nRT and TC neurons from intra-cortical injection experiments (data not shown).

Data acquisition and analysis. For data acquisition and analysis, we used a Digidata 1320 digitizer and pClamp9 (Molecular Devices). We amplified the signals with Multiclamp (Molecular Devices), and sampled and filtered them at 10 kHz. We detected and analyzed EPSCs with wDetecta, a custom postsynaptic current detection program (http://huguenardlab.stanford.edu/apps/wdetecta/). We calculated the amplitude of action potentials as the potential difference between their voltage threshold and the peak of the waveform. Numerical values are given as means ± s.e.m. unless stated otherwise. We assessed statistical significance by performing one-way ANOVA, the Mann-Whitney rank sum test or the Kolmogoroff-Smirnoff test. We performed statistical analyses with Sigma Stat 3.5 and Origin 7.0 (Microcal Software). For EPSCs ,we fitted the peak-to-baseline decay phase of the resulting current trace by the double exponential function $I = A_1 e^{-t/\tau_1} + A_2 e^{-t/\tau_2}$ (**Fig. 3d**), where A_1 and A_2 are the slow and fast amplitude components, and τ_1 and τ_2 are the slow and fast decay-time constants, respectively. We calculated the weighted decay-time constant ($\tau_{D,W}$) using the equation

$$\tau_{D,W} = \frac{\tau_1 A_1 + \tau_2 A_2}{A_1 + A_2}$$

48. Paz, J.T., Christian, C.A., Parada, I., Prince, D.A. & Huguenard, J.R. Focal cortical infarcts alter intrinsic excitability and synaptic excitation in the reticular thalamic nucleus. *J. Neurosci.* **30**, 5465–5479 (2010).
49. Dobrunz, L.E. & Stevens, C.F. Heterogeneity of release probability, facilitation, and depletion at central synapses. *Neuron* **18**, 995–1008 (1997).
50. Wong-Riley, M.T. Endogenous perioxidatic activity in brain stem neurons as demonstrated by their staining with diaminobenzidine in normal squirrel monkeys. *Brain Res.* **108**, 257–277 (1976).